RSC Advances

PAPER

View Article Online
View Journal | View Issue

Cite this: *RSC Adv.*, 2024, **14**, 2439

Two-photon excited luminescence of sulfur quantum dots for heavy metal ion detection

Agnieszka Siomra, Dominika Wawrzyńczyk, Marek Samoć and Marcin Nyk *

Spectrally-resolved third-order nonlinear optical properties of water-dispersed sulfur quantum dots (SQDs) were investigated in the wavelength range from 740 nm to 820 nm with the two-photon excited emission technique using a tunable femtosecond laser system. The maximum value of the two-photon absorption (TPA) cross-section (σ_2) for ~5.4 nm size SQDs was found to be 185 GM (Goeppert-Mayer unit), while the two-photon brightness ($\sigma_2 \times \eta$) was found to be 1.5 GM at 780 nm, the wavelength being in the first biological transmittance window. The TPA properties are presented here as appropriate cross-sections normalized per molecular weight which enables meaningful comparison of the nonlinear factors of the studied quantum dots with those of various nanomaterials. The optimized TPA properties of these hydrophilic colloidal SQDs may be potentially useful for detection of Fe^{3+} metal ions. The experimentally determined limit of Fe^{3+} detection for both one- and two-photon regime was 10 μmol L^{-1} (0.6 μg mL^{-1}). Förster resonance energy transfer between SQDs as donors and Fe^{3+} metal ions as acceptors was confirmed as one of the possible detection mechanisms using a time-correlated single photon counting technique.

Received 3rd November 2023
Accepted 6th January 2024

DOI: 10.1039/d3ra07521d

rsc.li/rsc-advances

Introduction

Heavy metal contamination is a major cause of concern due to the harmful impact it may have on the environment and human health. In addition to severe ecological consequences, exposure to excessive levels of metallic pollutants can result in developmental abnormalities, neurological conditions, and ultimately, cancer.[1–3] Therefore, there is a growing need for effective monitoring methods that allow highly sensitive and quick detection of heavy metal ions in real time. To date, a wide range of analytical techniques have been developed to facilitate the determination and quantification of heavy metals in samples, including atomic absorption spectroscopy, inductively coupled plasma mass spectroscopy, voltammetric methods, surface plasmon resonance, Raman spectroscopy and laser-induced breakdown spectroscopy.[4–8] Yet, these techniques often require specialized equipment, complex and time-consuming sample preparation, or fail to meet the satisfactory sensitivity and detection limits.[9]

The use of quantum dots (QDs) in heavy metal ion detection offers a promising approach for monitoring environmental pollution and safeguarding human health. Owing to their tunable optical properties, these zero-dimensional semiconductor nanoparticles can be efficiently utilized as fluorescent sensors, providing high sensitivity and selectivity, as well as rapid response to a variety of analytes.[10–13] One of the most researched classes of QDs are cadmium-based QDs (*e.g.* CdSe, CdTe, CdS). They attracted the attention of scientists due to their excellent optical characteristics, including broad absorption and narrow emission spectra, high quantum yields, excellent photostability and desirable nonlinear optical responses.[14–16] These properties make cadmium-based QDs attractive not only for sensing purposes, but also for optoelectronics, bioimaging and biodiagnostic applications.[17–21] However, despite their multifunctionality, the primary concern over potential toxicity resulting from the presence of the heavy metal in the chemical composition severely limits the practical application of QDs based on cadmium.[22] Consequently, metal-free nanomaterials are being explored as a more suitable alternative for the use as nanoprobes, sensors or biomarkers. Recently, sulfur quantum dots (SQDs) have aroused great interest, as they possess favorable optical properties and exhibit low toxicity, high biocompatibility, antimicrobial activity and excellent water dispersibility.[23–25] As a result, SQDs have emerged also as highly promising materials in the field of optical based sensing. Leveraging their fluorescence properties, SQDs can be effectively employed as nanosensors for metal ions or certain organic molecules. In 2019, Wang *et al.* demonstrated an aggregation-caused quenching of SQDs fluorescence in the presence of Co^{2+} and proposed an SQDs-Co^{2+} based sensing platform for determination of nofloxacin.[26] Similarly, Tan *et al.* used blue fluorescent SQDs for the highly sensitive and selective determination of Cr(VI) and ascorbic acid.[27] In 2021, Huang *et al.* reported that SQDs display selective fluorescence quenching

Institute of Advanced Materials, Faculty of Chemistry, Wrocław University of Science and Technology, Wyb. Wyspianskiego 27, PL-50370, Wrocław, Poland. E-mail: marcin.nyk@pwr.edu.pl

behavior towards Fe^{3+} and phytic acid.[28] A year later, Ma *et al.* employed SQDs to detect alkaline phosphatase in serum samples.[29] Furthermore, fluorescent probes based on SQDs were also successfully employed for rapid and sensitive detection of copper, lead, bismuth and mercury ions.[12,30,31] The development of SQDs as sensors remains an active area of research and different strategies to enhance the stability, sensitivity, and selectivity of SQDs for detection purposes are still being explored. On the other hand, significant efforts are nowadays put on developing two-photon active sensors since they offer substantial advantages that can contribute to improved detection capabilities, particularly valuable in biomedical research, diagnostics and environmental monitoring. Functioning of such sensors utilizes the principle of two-photon absorption (TPA), which is a nonlinear optical (NLO) process where two photons of low energy are simultaneously absorbed by a material *via* a virtual state, resulting in the excitation of electrons to higher energy levels. Employing two-photon active nanomaterials, operating at relatively long excitation wavelengths falling in the range of the near-infrared (NIR) biological window, minimizes the risk of photodamage and/or photobleaching, and at the same time increases the penetration depth with a high contrast in, *e.g.*, highly scattering media such as biological samples. Thus far, the NLO characteristics of SQDs have been presented only sparsely in the literature. In 2021, Xu *et al.* reported the SQDs as saturable absorbers with nonlinear absorption coefficient of 5.89×10^{-2} cm GW^{-1} for applications as a mode locker in fiber lasers for generation of ultrafast laser pulses.[32] The application of SQDs synthesized from *S*-ethylenediamine solution in two-photon fluorescence imaging was demonstrated for the first time by Gao *et al.* in 2022.[33] A few months later, Tan *et al.* reported dendritic SQDs functionalized with hyperbranched polyglycerol for two-photon fluorescence imaging and the detection of hydroxyl radicals and ascorbic acid.[34]

In this work, we demonstrate in the quantitative manner the ability of SQDs to exhibit NLO response in an expanded spectral range of wavelengths, which has not been described in the literature before. The results shed light on the potential applicability of this nanomaterial as two-photon excited luminescence based sensor for metal ions detection – including heavy metal ions. Fe^{3+} ions were selected as the model ions to evaluate the sensing capability of SQDs. The detection and quantification of ferric ions holds significance for several reasons. Their concentration can provide valuable details for water quality assessment. By monitoring and quantifying ferric ions, it becomes possible to identify the occurrence of contaminants, pollutants, or other phenomena that affect water quality. Moreover, ferric ions play a crucial role not only in environmental processes but also in biological systems, including humans. Both deficiency and excess of these ions can lead to iron-related diseases, including anaemia or hemochromatosis.[35] Several fluorescent nanomaterials have been proposed as effective Fe^{3+} sensors, including SQDs.[28,36,37] However, the ability of SQDs to sense ferric ions in the two-photon regime remains unexplored in the existing literature. This particular property of SQDs holds significant importance, especially in the context of ion sensing within biological systems. This study also confirms that SQDs could represent a promising alternative to the nonlinear absorbers currently used as markers for nonlinear microscopy.

Experimental

Materials

Sublimed sulfur, sodium hydroxide (semiconductor grade), poly(ethylene glycol) 400 and iron(III) chloride hexahydrate were purchased from Merck (Sigma Aldrich). Milli-Q Type 1 Ultrapure water (resistivity 18.2 MΩ cm at 25 °C) was used in all experiments.

Synthesis of SQDs

SQDs were synthesized using the microwave-assisted method described previously by Xiao *et al.* with some changes.[38] Briefly, 0.3 g of sublimed sulfur, 0.8 g of sodium hydroxide, 0.5 mL of poly(ethylene glycol) and 10 mL of ultrapure water were mixed on a magnetic stirrer until complete dissolution of NaOH pellets. The reaction mixture was then transferred into a Teflon-lined reaction vessel and placed in a microwave reactor (MAGNUM II, ERTEC – Poland) set at 170 °C for 4 h. The light-yellow SQDs aqueous solution was stored at room temperature for further studies.

Preparation of Fe^{3+} solution

50 mg of $FeCl_3 \cdot 6H_2O$ and 18.5 mL of ultrapure water were mixed on a magnetic stirrer for 10 minutes. The obtained 10 mM stock solution of ferric ions was stored at room temperature for further studies.

Methods

Morphology and chemical composition

The morphology and elemental composition of the prepared SQDs was investigated with a FEI Tecnai G^2 20 X-TWIN transmission electron microscope, equipped with energy-dispersive X-ray spectrometer. Samples were prepared by dropping diluted SQDs solution onto copper grids, with subsequent solvent evaporation.

Optical characterization

The absorption spectra of the obtained colloidal SQDs were measured using a JASCO® V-670 UV-vis spectrophotometer. The one-photon excited emission spectra of the studied QDs were registered using a HORIBA® FluoroMax-4 spectrofluorometer. The NLO characteristics were determined utilizing tunable ~55 femtosecond laser pulses at the repetition rate of 1 kHz, supplied from the Coherent Astrella® ultrafast regenerative amplifier operating as the 800 nm pump, followed by the TOPAS-PRIME manufactured by Light Conversion® a parametric amplifier providing wavelengths in the range from 600 to 1500 nm. Two-photon excited emission spectra were measured using an Ocean Insight Flame CCD fiber-optic spectrometer with dedicated software. The quantitative determination of two-

photon absorption cross-sections of SQDs was based on comparison between the emission intensities of the studied nanomaterials and the corresponding reference emission intensities of Coumarin 153 dye solution, following the two-photon excited emission method (TPEE) as described by Makarov *et al.*[39] The photoluminescence quantum yields (η) of SQDs and reference dye were measured by the integrating sphere method using a 377 nm laser diode (Becker & Hickl, BDL-377-SMC) as the excitation source and an Ocean Insight Flame CCD fiber-optic spectrometer with dedicated software. The luminescence lifetimes were measured using the Time Correlated Single Photon Counting (TCSPC) method and a Becker & Hickl system constructed from a TCSPC module (SPC-130-EM) and a hybrid PMT detector (HPM-100-06) with a detector control card (DCC 100) mounted to the Princeton Instruments® spectrograph (Acton SpectraPro-2300i) under excitation with a picosecond $\lambda = 377$ nm laser diode (BDL-377-SMC) with repetition rate of 20 MHz. For two-photon excited luminescence ion sensing, the beam of the same tunable femtosecond laser with a proper wavelength (at the wavelength of the maximum cross-section σ_2 and maximum two-photon brightness – $\sigma_2 \times \eta$) was focused by the lens onto the colloidal samples contained in a quartz-cuvette with a path length of 1 cm. The emission from the samples was collected perpendicularly to the excitation laser beam by a pair of lenses and an optical fiber that was connected to a CCD camera (Ocean Insight Flame). A cut-off short-pass filter with a wavelength of 750 nm was placed before the CCD collimator to minimize the emission from scattering of the excitation laser beam. To avoid white-light continuum generation the laser intensity was adjusted with the proper neutral-density filter. Various amounts of ferric ions colloidal stock solution were then added to 1 mL of SQDs water solution and kept for 5 min before each step of the measurements.

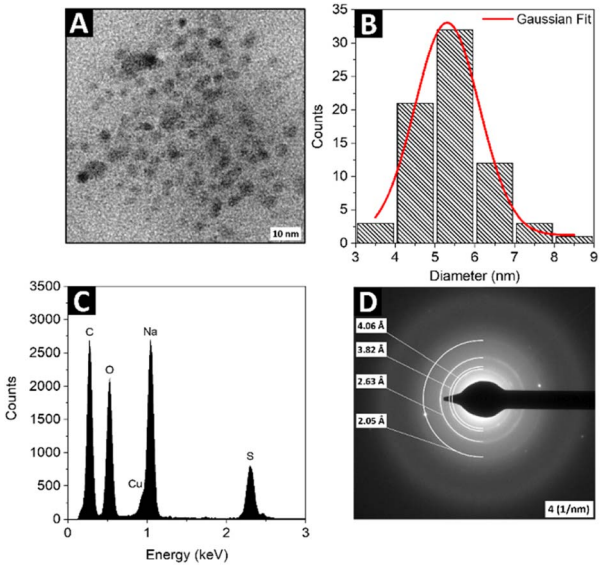

Fig. 1 The representative TEM image (A) and its size distribution histogram (B) of the SQDs sample; the EDX spectra (C) and SAED (D) of the SQDs sample.

Results and discussion

Morphological analysis and characterization

Fig. 1 shows a representative transmission electron microscope (TEM) image (panel A) and the respective size distribution histogram of the synthesized colloidal SQDs sample (panel B). The SQDs exhibit good monodispersity and appear spherical in shape, with average diameter of 5.4 ± 0.9 nm. Energy-dispersive X-ray (EDX) spectroscopy was conducted to determine the elemental composition of the investigated nanomaterial. As shown in Fig. 1C, the EDX spectrum confirms that the SQDs are composed mainly of S, C, O. Here it is to be noted, that the presence of C and O is attributed to the PEG ligand surrounding the sulfur core, while Na originates from the precursor and Cu comes from the copper grid used for the TEM imaging and analysis. The selected area electron diffraction (SAED) pattern of the particles (Fig. 1D) matched favorably with *d*-spacing values lines 4.06 Å, 3.82 Å, 2.63 Å and 2.05 Å, the standard lines of pure orthorhombic sulfur determined by X-ray diffraction studies.[40]

Optical properties

To explore linear optical properties of the colloidal SQDs, the UV-vis absorption and luminescence emission spectra were investigated. Fig. 2A shows the absorption spectrum of synthesized SQDs. The single strong absorption band is observed at 360 nm and can be assigned to the existence of S_8^{2-}

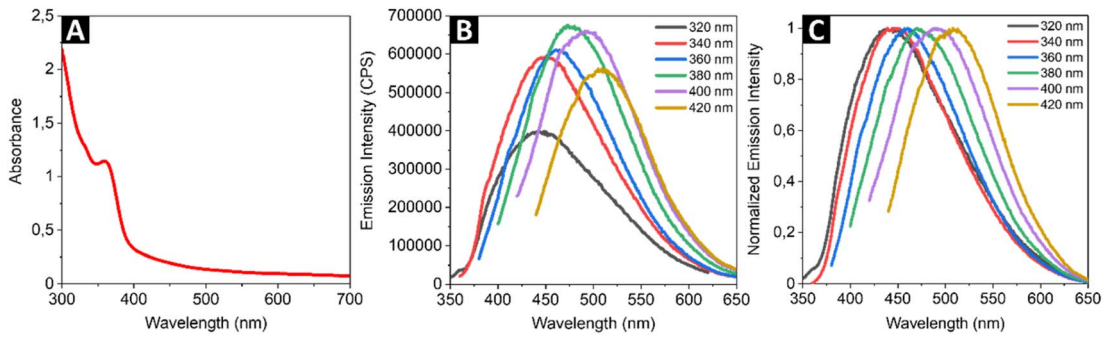

Fig. 2 The absorption (A), luminescence (B) and normalized luminescence emission spectra of the SQDs under different excitation wavelengths (C).

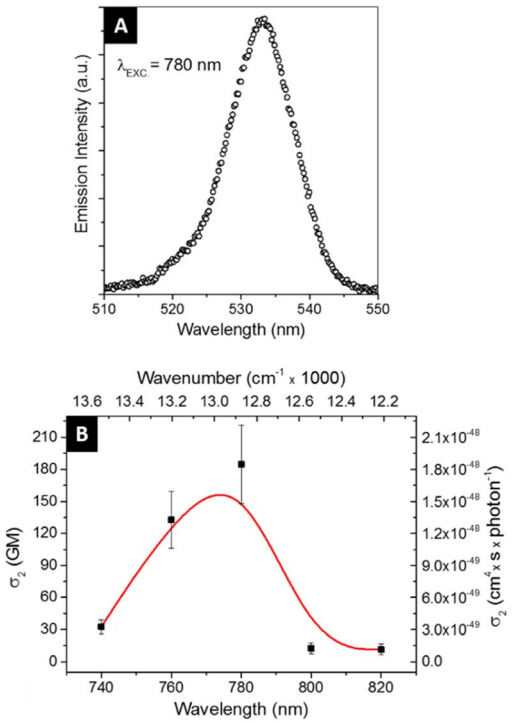

Fig. 3 Example of two-photon induced emission of SQDs upon excitation with 780 nm femtosecond laser (A) and wavelength dependence of TPA cross-sections of the SQDs determined by TPEE method (B). The red line is drawn to guide the eyes.

adsorbed on the surface of SQDs, similar to the cases of samples reported by Wang and co-workers.[41] As shown in Fig. 2B, the SQDs exhibit different emission intensities when excited at different wavelengths. The excitation wavelength of 380 nm was found to yield the highest emission intensity. The normalized emission spectrum of the SQDs (Fig. 2C) illustrates the red-shift of the emission peak following an increase in the excitation wavelength, which is in good agreement with previous works.[41,42] The excitation-dependent behavior can be attributed to the synergistic effect of the size of SQDs and surface states.[43] Due to the limited literature on NLO behavior of the SQDs, the two-photon excited emission (Fig. 3A) properties of the nanomaterial were measured in an expanded (from 740 nm to 820 nm) range of excitation wavelengths compared to previous studies. We used the two-photon excited emission technique, as described by Makarov *et al.*[39] to determine the values of two-photon absorption (TPA) cross-sections σ_2 based on the emissive properties of the studied SQDs. The wavelength dependence of the calculated σ_2 is shown in Fig. 3B. The maximum TPA cross-section value was found to be 185 GM (Goeppert-Mayer units, where 1 GM = 10^{-50} cm^4 s per photon) upon excitation at 780 nm. Scaling this value with the molecular weight (MW) of a single SQD particle gives the σ_2/MW parameter equal to 1.8×10^{-3} GM mol g^{-1}. The peak values of TPA cross-sections of the SQDs determined through TPEE experiments were compared to the peak values of TPA cross-sections of other emerging nanomaterials and are presented in Table 1. In order for a material to be useful in bioimaging through two-photon excitation, it should satisfy certain criteria. A two-photon probe for biological targets should exhibit desirable characteristics such as excellent water solubility, high specificity towards the intended target, and exceptional photostability, as well as possess a considerable two-photon action cross-section often called two-photon brightness ($\sigma_2 \times \eta$). It the case of the currently studied SQDs, which due to the selected synthetic method formed stable water solutions, the combination of the measured σ_2 and η values gives a moderately high result for the two-photon action cross section, thus showing this type of material to be an interesting candidate for future investigations (*i.e.*, synthesis parameters optimization, modification of composition) to further increase those values. To enable a better comparison of the NLO properties, the TPA cross-sections of the SQDs were normalized by dividing them by molecular weight to obtain σ_2/MW and two-photon action cross-sections ($\sigma_2 \times \eta$) were also calculated. The first quantity is relevant for comparing different types of two-photon absorbers, while the latter for assessing the two-photon brightness available from an individual optical marker for nonlinear imaging techniques. The σ_2/MW values obtained for SQDs were similar to the corresponding factors obtained by us for CdSe–Au NPs[45] and InP@ZnS QDs[46] and two orders of magnitude smaller than those for CdSe QDs. On the other hand, the investigated cadmium-free SQDs showed only slightly lower $\sigma_2 \times \eta$ values than conventional fluorescent probes now in use, which were on the level of the corresponding values reported for organic

Table 1 Comparison of the maximum values of the two-photon absorption cross-sections (σ_2), molecular weight normalized two-photon absorption cross-sections (σ_2/MW), quantum yields (η) and two-photon action cross-sections ($\sigma_2 \times \eta$) of selected nanoparticles and Coumarin 153 as a reference dye for TPEE method

Material (size)	Solvent	Technique	λ_{exc} [nm]	σ_2 [GM]	σ_2/MW [GM mol g^{-1}]	η [%]	$\sigma_2 \times \eta$ [GM]	Ref.
SQDs from NaOH precursor (~5.6 nm)	Water	TPEE	780	185	1.8×10^{-3}	0.8	1.5	This work
SQDs from EDA precursor (~3.5 nm)	Water	TPEE	800	16×10^3	0.57	87.8	14×10^3	33
Porous silicon NPs (~60 nm)	Water	TPEE	800	25	—	22.3	5.6	44
Hybrid CdS–Au NPs (~20 nm)	Water	TPEE	725	15.8×10^3	20×10^{-3}	10	1.58×10^3	45
Core–shell InP@ZnS QDs (~4.3 nm)	Toluene	Z-scan	880	2200	18×10^{-3}	31	682	46
Tetraphenylethylene-PSMA NPs (~64.1 nm)	Water	TPEE	1040	28	—	75	21	47
Coumarin 153	CCl_4	TPEE	800	45	0.15	25.6	11.5	39, this work

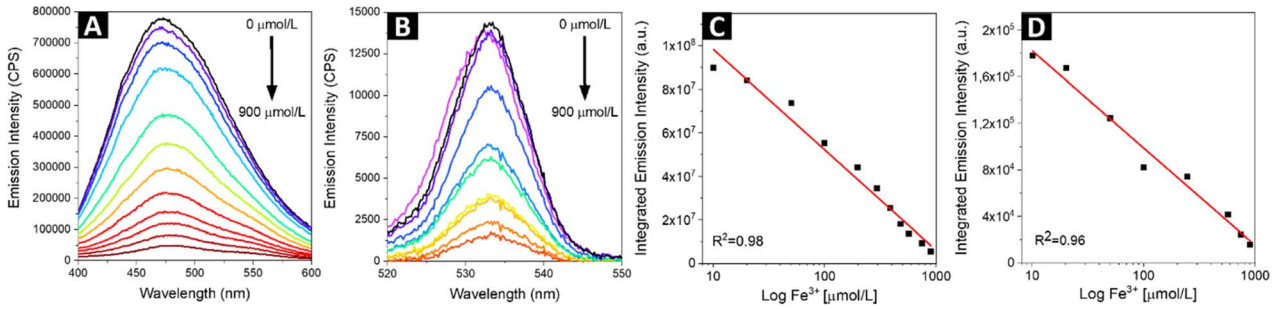

Fig. 4 The one-photon (A) and two-photon (B) excited emission spectra of SQDs solution at excitation wavelengths of 380 nm and 780 nm, respectively, demonstrating the emissions quenching upon increasing concentration of Fe^{3+} ions. The relationship between the integrated one-photon (C) and two-photon (D) fluorescence intensities *versus* Fe^{3+} concentration.

molecules designed specifically for enhanced two-photon absorption.[48] We must also remark that recently Gao *et al.* conducted a single wavelength (800 nm) NLO study of a similar SQDs system.[33] Those authors reported a high two-photon cross-section of 16×10^3 GM; however, not much detail has been provided regarding the measurement method and the calculation of the relevant parameters. The above paper demonstrates the use of the SQDs as efficient markers for multi-photon microscopy, which establishes this type of nano-materials as non-toxic alternative for cadmium-based QDs in bioimaging applications. In comparison to the single-photon excited luminescence observed at ~475 nm under the 380 nm excitation, the TPEE peaked at 533 nm under the 780 nm fs laser excitation (see: Fig. 4A and B). This corresponds to a redshift of 58 nm (0.29 eV) in relation to the single-photon excited luminescence. The origin of the redshift in the TPEE spectrum can be postulated to arise from two possible mechanisms: either a preferential absorption of two photons simultaneously leading to transitions to trap states or preferential excitation of larger particles. In both scenarios, when single-photon excitation occurs, the primary emission is from the exciton state, with some additional contribution from trap-state emission. Yet, when the energy of the photons involved in the two-photon excitation process are closely aligned with the energy levels of the trap states, or when larger-sized nanoparticles play a dominant role, the intensity of trap-state emission increases in comparison to exciton emission. This results in a shift toward longer wavelengths in the overall emission spectrum.[49,50]

Fluorescence sensing of Fe^{3+}

For metal sensing, various amounts of stock ferric ion solution were introduced to 1 mL of aqueous dispersion of SQDs resulting in various concentrations of Fe^{3+} in the range from 0 to 900 μmol L^{-1}. The samples were mixed for a few seconds and the emission response in one-photon and two-photon regime was recorded for excitation wavelengths of 380 nm and 780 nm, respectively (Fig. 4A and B). In both cases the fluorescence intensity of SQDs showed a continuous decrease as the concentration of Fe^{3+} in the investigated sample was increasing. The experimentally determined limit of detection (LOD) for both one- and two-photon regime was found to be 10 μmol L^{-1}. As shown in Fig. 4C and D, the signal ratio shows good linearity with Fe^{3+} concentration in the range of 0 to 900 μmol L^{-1}. In Table 2, parameters of Fe^{3+} detection of as-obtained SQDs are compared to parameters reported for other nanoprobes, including SQDs synthesized under different conditions. It is important to note that while SQDs presented in this work offer remarkable features, QDs-based sensors with superior detection range and LOD have been already proposed. However, the research landscape regarding two-photon active sensors for Fe^{3+} detection remains limited, with a small number of studies conducted thus far. Hence, this study represents a significant contribution as it describes, for the first time, the utilization of SQDs for ferric ions detection under two-photon excitation at NIR region of wavelengths. Besides changes in emission intensity in response to the heavy metal ions presence, which can be prone to errors connected with SQDs concentration fluctuations or changes in excitation intensity, widely used in analytical strategies based on QDs for heavy metal ions detection is Förster Resonance Energy Transfer (FRET),

Table 2 Comparison of Fe^{3+} detection parameters of selected QDs-based nanoprobes

Material	Regime	Detection range [μmol L^{-1}]	LOD [μmol L^{-1}]	Ref.
SQDs (hydrothermal method)	One-photon, two-photon	10–900	10	This work
SQDs (synthesized under O_2 atmosphere)	One-photon	0.1–300	0.102	28
PVA-capped SQDs	One-photon	0.09–165	0.092	36
SQDs (30 h reaction time)	One-photon	0.05–700	0.0536	37
Single-layer graphene QDs	One-photon	0.26–85	0.26	51
Tungsten oxide QDs	One photon	2.6–1000	2.69	52
Nitrogen-doped carbon dots	One-photon, two-photon	0.001–300, 0.002–150	1.56×10^{-3}, 2.21×10^{-3}	53

a nonradiative energy transfer mechanism generated in close proximity between donor – fluorophores – and acceptor – metal ions.[54] For example, upon adding Hg^{2+}, the fluorescence of both the CdTe QDs (donor) and butyl-rhodamine B (acceptor) was quenched, but the quenching of the acceptor was much greater.[55] Additionally, a FRET system mechanism with electrostatic interactions between the positively charged CdTe QDs capped with cysteamine and the negatively charged Au NPs capped with 11-mercaptoundecanoic acid was reported.[56] The authors described that this system had a detection limit of 30 ppb and was used for determination of Pb^{2+} content based on FRET mechanism between CdTe QDs and Au NPs in the presence of Pb^{2+}. In our study, we observe a nonradiative energy transfer process occurring between the SQDs (donor) and Fe^{3+} ions (acceptor). The potential mechanism of the fluorescence quenching has been already proposed.[28] Due to the presence of hydroxyl groups originating from PEG, SQDs form a complex with Fe^{3+}. This complex formation is associated with nonradiative electron transfer, resulting in the quenching of the fluorescence of SQDs. To determine whether the observed luminescence of SQDs was caused by nonradiative energy transfer, like in the case of the Förster mechanism, fluorescence lifetimes of SQDs were measured using time-correlated single photon counting technique during the sequential addition of Fe^{3+} ions containing solution (starting from 0 μl up to 200 μl). The measured decay curves were fitted with double exponential model, and the exact values of lifetimes short and long components (together with percentage in mean lifetime values) are collected in Table 3, while the evolution of mean decay τ values in response to the addition of ferric solution is summarized in Fig. 5A. The representative traces of the luminescence decays measured at 475 nm (maximum of the SQDs luminescence) are shown in Fig. 5B. There is a noticeable decrease in the luminescence decay time of the SQDs (donor) upon addition of metal ions (acceptor), which suggests energy transfer through nonradiative dipole–dipole coupling. The mean lifetime of emission for raw SQDs in water is approximately 1.42 ns, which decreases to 1.12 ns upon the addition of a maximum of 200 μL of ferric ions solution. To further quantify the presence of FRET one can determine the transfer efficiency Φ_{ET}, based on the variation in the lifetimes, from the lifetime measurements of the donor – SQDs – in the absence (τ_D) and presence (τ_{DA}) of the acceptor – ferric ions – as:[57]

$$\Phi_{ET} = 1 - \frac{\tau_{DA}}{\tau_D} \quad (1)$$

According to decay measurements, the energy transfer efficiency increases with the concentration of Fe^{3+} solution and varies from *ca.* 4.9% to 21.6%. It is evident that the physical mixing of solutions of SQDs and Fe^{3+} results in sufficient physical contact between the donor and the acceptor that the FRET for metal ions detection becomes possible. However, it should be taken into account that quenching is actually any process that decreases the fluorescence intensity and, as such, may be the result of a variety of mechanisms. The decrease in fluorescence intensity and lifetime shortening do not, in fact, differentiate between energy transfer and electron transfer because both processes can cause fluorescence intensity decrease and lifetime shortening. In principle, fluorescence quenching of an emitter in a similar system can occur *via* various kinds of mechanisms, such as static or dynamic quenching, inner filter effect, and electron-energy transfer.[58]

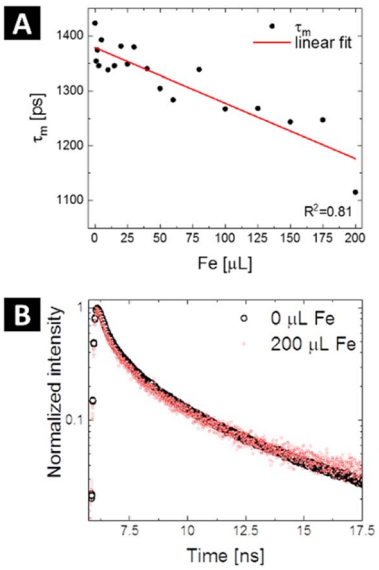

Fig. 5 Calculated mean PL lifetimes of SQDs as a function of the detection amount of Fe^{3+} – black dots – with fitting showing a linear trend (A) and time-resolved PL decay curves of the SQDs recorded before (black) and after addition of 200 μL of Fe^{3+} solution (red) (B).

Table 3 Calculated luminescence lifetime values (short and long components, together with mean values) for SQDs upon sequential addition of ferric ions solution

Amount of Fe^{3+} [μL]	τ_1 [ps], A_1 [%]	τ_2 [ps], A_2 [%]	τ_m [ps]
0	611 (80.79%)	4837 (19.21%)	1422.92
1	585 (81.11%)	4652 (18.89%)	1353.81
2	608 (81.64%)	4779 (18.36%)	1373.72
3	580 (81.34%)	4678 (18.66%)	1345.13
5	627 (81.73%)	4814 (18.27%)	1392.38
10	580 (81.57%)	4689 (18.43%)	1337.66
15	583 (81.30%)	4661 (18.70%)	1345.20
20	619 (81.96%)	4840 (18.04%)	1380.96
25	582 (81.34%)	4690 (18.66%)	1348.63
30	618 (81.85%)	4815 (18.15%)	1379.36
40	575 (81.15%)	4632 (18.85%)	1340.06
50	559 (81.27%)	4538 (18.73%)	1304.28
60	548 (81.43%)	4510 (18.57%)	1283.52
80	577 (81.07%)	4599 (18.93%)	1338.52
100	536 (81.16%)	4417 (18.84%)	1267.13
125	528 (80.81%)	4383 (19.19%)	1268.18
150	497 (79.46%)	4134 (20.54%)	1243.58
175	507 (80.00%)	4206 (20.00%)	1247.24
200	419 (79.21%)	3771 (20.79%)	1115.50

Conclusions

In conclusion, we have successfully demonstrated the ability of SQDs to exhibit nonlinear optical responses in the range of excitation wavelengths 740–820 nm. Quantitative evaluation of TPA cross-sections of as-obtained SQDs led to values as high as 185 GM. To the best of our knowledge, this is the first report demonstrating TPA cross-sections of SQDs values in an expanded excitation wavelength range. Furthermore, the potential applicability of SQDs as two-photon active optical sensors for metal ions was investigated. We explored the sensitivity of SQDs to Fe^{3+} in both one-photon and two-photon regime, revealing the fluorescence quenching based detection of metal ions. Experimentally established LOD for both regimes was approximately 10 μmol L^{-1}. It's worth noting that for water quality assessment applications, the detection limit for Fe^{3+} should be lower than the maximum allowable concentration of iron in drinking water, which according to the Directive 2020/2184 of the European Parliament and of the Council of 16 December 2020 on the quality of water intended for human consumption is set at ~3.6 μmol L^{-1} (0.2 mg L^{-1}). Overall, this study contributes to the existing knowledge about SQDs by providing an analysis of their nonlinear optical behavior. The findings of this research can serve as a foundation for further investigations and offer new avenues for the development of novel nanomaterials based on SQDs for sensing applications in nonlinear photonics and biophotonics.

Data availability

The data that supports the findings of this study is available from the corresponding authors upon reasonable request.

Author contributions

Agnieszka Siomra: formal analysis, investigation, data curation, writing – original draft. Dominika Wawrzyńczyk: investigation, data curation, writing – original draft. Marek Samoć: investigation, writing – review & editing. Marcin Nyk: conceptualization, methodology, writing – review & editing, supervision, project administration, funding acquisition.

Conflicts of interest

The authors declare that they have no known competing financial interests or personal relationships that could have appeared to influence the work reported in this paper.

Acknowledgements

The work was founded by the National Science Centre, Poland, under Grant UMO-2018/30/E/ST5/00718.

References

1 J. Briffa, E. Sinagra and R. Blundell, *Heliyon*, 2020, **6**, e04691.
2 S. Caito and M. Aschner, Chapter 11 – Neurotoxicity of metals, *Handbook of Clinical Neurology*, Elsevier, 2015.
3 F. Gorini, F. Muratori and M. A. Morales, *Review Journal of Autism and Developmental Disorders*, 2014, **1**, 354–372.
4 W. Daniya, S. Saleviter and Y. W. Fen, *Sens. Mater.*, 2018, **30**, 2023–2038.
5 M. T. Jin, H. Yuan, B. Liu, J. J. Peng, L. P. Xu and D. Z. Yang, *Anal. Methods*, 2020, **12**, 5747–5766.
6 L. A. Malik, A. Bashir, A. Qureashi and A. H. Pandith, *Environ. Chem. Lett.*, 2019, **17**, 1495–1521.
7 C. D. Metcalfe, T. Sultana, J. Martin, K. Newman, P. Helm, S. Kleywegt, L. Shen and V. Yargeau, *Environ. Monit. Assess.*, 2018, **190**, 555.
8 Z. L. Sun, J. J. Du and C. Y. Jing, *J. Environ. Sci.*, 2016, **39**, 134–143.
9 J. A. Buledi, S. Amin, S. I. Haider, M. I. Bhanger and A. R. Solangi, *Environ. Sci. Pollut. Res.*, 2021, **28**, 58994–59002.
10 H. Z. Jiao, L. Zhang, Z. H. Liang, G. H. Peng and H. W. Lin, *Microchim. Acta*, 2014, **181**, 1393–1399.
11 P. Sharma and M. S. Mehata, *Mater. Res. Bull.*, 2020, **131**, 110978.
12 X. Wang, W. Guo, X. Wang, Q. Hua, F. Tang, X. Li, F. Luan, Z. Zhang, C. Tian, X. Zhuang and L. Zhao, *Arabian J. Chem.*, 2022, **15**, 104080.
13 D. Wawrzynczyk, J. Szeremeta, M. Samoc and M. Nyk, *Sens. Actuators, B*, 2017, **252**, 483–491.
14 M. A. Antoniak, J. Grzyb and M. Nyk, *J. Lumin.*, 2019, **209**, 57–60.
15 D. Mo, L. Hu, G. M. Zeng, G. Q. Chen, J. Wan, Z. G. Yu, Z. Z. Huang, K. He, C. Zhang and M. Cheng, *Appl. Microbiol. Biotechnol.*, 2017, **101**, 2713–2733.
16 F. Zhang, D. M. Yi, H. Z. Sun and H. Zhang, *J. Nanosci. Nanotechnol.*, 2014, **14**, 1409–1424.
17 S. Bin Hafiz, M. Scimeca, A. Sahu and D. K. Ko, *Nano Convergence*, 2019, **6**, 7.
18 J. M. Gillies, *Inorg. Chim. Acta*, 2019, **495**, 119001.
19 W. C. Law, K. T. Yong, I. Roy, H. Ding, R. Hu, W. W. Zhao and P. N. Prasad, *Small*, 2009, **5**, 1302–1310.
20 L. S. Li, Z. Q. Zhang, Y. B. Zhang, Y. F. Liu and M. X. Zhao, *Mater. Des.*, 2022, **220**, 110890.
21 M. M. Rahman, M. R. Karim, H. F. Alharbi, B. Aldokhayel, T. Uzzaman and H. Zahir, *Chem.–Asian J.*, 2021, **16**, 902–921.
22 N. Chen, Y. He, Y. Y. Su, X. M. Li, Q. Huang, H. F. Wang, X. Z. Zhang, R. Z. Tai and C. H. Fan, *Biomaterials*, 2012, **33**, 1238–1244.
23 K. K. Ning, Y. J. Sun, J. X. Liu, Y. Fu, K. Ye, J. G. Liang and Y. Wu, *Molecules*, 2022, **27**, 2822.
24 A. Pal, F. Arshad and M. P. Sk, *Adv. Colloid Interface Sci.*, 2020, **285**, 102274.
25 H. Ruan and L. Zhou, *Front. Bioeng. Biotechnol.*, 2022, **10**, 909727.
26 S. Wang, X. Bao, B. Gao and M. Li, *Dalton Trans.*, 2019, **48**, 8288–8296.
27 Q. Tan, X. X. An, S. Pan, H. Liu and X. L. Hu, *Spectrochim. Acta, Part A*, 2021, **247**, 119122.

28 Z. M. Huang, Y. Gao, Z. Y. Huang, D. L. Chen, J. H. Sun and L. Zhou, *Microchem. J.*, 2021, **170**, 106656.
29 F. H. Ma, Q. Zhou, M. H. Yang, J. L. Zhang and X. Chen, *Nanomaterials*, 2022, **12**, 2787.
30 A. Q. Huang, X. F. Yang, T. Xia, D. C. He, R. Zhang, Z. T. Li, S. C. Yang, Y. Liu and X. D. Wen, *Microchem. J.*, 2022, **179**, 107639.
31 S. K. Tammina, R. Priyadarshi and J. W. Rhim, *New J. Chem.*, 2023, **47**, 7733–7745.
32 N. Xu and Q. Wen, *Opt. Laser Technol.*, 2021, **138**, 106858.
33 P. X. Gao, Z. Y. Huang, J. S. Tan, G. S. Lv and L. Zhou, *ACS Sustain. Chem. Eng.*, 2022, **10**, 4634–4641.
34 J. S. Tan, Y. H. Song, X. J. Dai, G. Wang and L. Zhou, *Nanoscale Adv.*, 2022, **4**, 4035–4040.
35 H. Harigae, *Int. J. Hematol.*, 2018, **107**, 5–6.
36 J. H. Lei, Z. M. Huang, P. X. Gao, J. H. Sun and L. Zhou, *Part. Part. Syst. Charact.*, 2021, **38**, 2000332.
37 Y. F. Liu, X. W. Shao, Z. J. Gao, X. L. Zhu, Z. C. Pan, Y. P. Ying, J. P. Yang, W. Pei and J. Wang, *J. Lumin.*, 2023, **257**, 119693.
38 L. Xiao, Q. C. Du, Y. Huang, L. Wang, S. J. Cheng, Z. Wang, T. N. Wong, E. K. L. Yeow and H. D. Sun, *ACS Appl. Nano Mater.*, 2019, **2**, 6622–6628.
39 N. S. Makarov, M. Drobizhev and A. Rebane, *Opt. Express*, 2008, **16**, 4029–4047.
40 A. G. Pinkus, J. S. Kim, J. L. McAtee and C. B. Concilio, *J. Am. Chem. Soc.*, 1959, **81**, 2652–2654.
41 H. G. Wang, Z. G. Wang, Y. Xiong, S. V. Kershaw, T. Z. Li, Y. Wang, Y. Q. Zhai and A. L. Rogach, *Angew. Chem., Int. Ed.*, 2019, **58**, 7040–7044.
42 L. H. Shen, H. N. Wang, S. N. Liu, Z. W. Bai, S. C. Zhang, X. R. Zhang and C. X. Zhang, *J. Am. Chem. Soc.*, 2018, **140**, 7878–7884.
43 Y. Y. Zang, J. X. Xu, Z. T. Lu, C. H. Yi and F. Y. Yan, *Colloids Surf., A*, 2022, **648**, 129361.
44 D. Kim, J. Kang, T. Wang, H. G. Ryu, J. M. Zuidema, J. Joo, M. Kim, Y. Huh, J. Jung, K. H. Ahn, K. H. Kim and M. J. Sailor, *Adv. Mater.*, 2017, **29**, 1703309.
45 K. C. Nawrot, D. Wawrzynczyk, O. Bezkrovnyi, L. Kepinski, B. Cichy, M. Samoc and M. Nyk, *Nanomaterials*, 2020, **10**, 715.
46 D. Wawrzynczyk, J. Szeremeta, M. Samoc and M. Nyk, *APL Mater.*, 2015, **3**, 116108.
47 N. Alifu, X. Dong, D. Li, X. Sun, A. Zebibula, D. Zhang, G. Zhang and J. Qian, *Mater. Chem. Front.*, 2017, **1**, 1746–1753.
48 B. Osmialowski, E. F. Petrusevich, K. C. Nawrot, B. K. Paszkiewicz, M. Nyk, J. Zielak, B. Jedrzejewska, J. M. Luis, D. Jacquemin and R. Zalesny, *J. Mater. Chem. C*, 2021, **9**, 6225–6233.
49 W. Chen, A. G. Joly and D. E. McCready, *J. Chem. Phys.*, 2005, **122**, 224708.
50 H. D. Ha, M. H. Jang, F. Liu, Y. H. Cho and T. S. Seo, *Carbon*, 2015, **81**, 367–375.
51 H. A. Wang, X. X. Wu, W. L. Dong, S. L. Lee, Q. H. Yuan and W. Gan, *Spectrochim. Acta, Part A*, 2020, **226**, 117626.
52 Y. Zhan, Y. L. Liu, Q. Q. Liu, Z. M. Liu, H. Y. Yang, B. F. Lei, J. L. Zhuang and C. F. Hu, *Sens. Actuators, B*, 2018, **255**, 290–298.
53 P. Lesani, G. Singh, C. Viray, Y. Ramaswamy, D. Zhu, P. Kingshott, Z. F. Lu and H. Zreiqat, *ACS Appl. Mater. Interfaces*, 2020, **12**, 18395–18406.
54 M. Vazquez-Gonzalez and C. Carrillo-Carrion, *J. Biomed. Opt.*, 2014, **19**, 101503.
55 J. Li, F. Mei, W. Y. Li, X. W. He and Y. K. Zhang, *Spectrochim. Acta, Part A*, 2008, **70**, 811–817.
56 X. Wang and X. Q. Guo, *Analyst*, 2009, **134**, 1348–1354.
57 M. Nyk, K. Palewska, L. Kepinski, K. A. Wilk, W. Strek and M. Samoc, *J. Lumin.*, 2010, **130**, 2487–2490.
58 D. P. Damera, R. Manimaran, V. V. K. Venuganti and A. Nag, *ACS Omega*, 2020, **5**, 19905–19918.